# Elucidating molecular-scale principles governing the anchoring of liquid crystal mixtures on solid surfaces

Jake I. Gold<sup>1‡</sup>, Jonathan K. Sheavly<sup>1‡</sup>, Nanqi Bao<sup>2‡</sup>, Huaizhe Yu<sup>2</sup>, Juriti Rajbangshi<sup>1</sup>, James J. Schauer<sup>1,3</sup>, Victor M. Zavala<sup>1</sup>, Nicholas L. Abbott<sup>2,\*</sup>, Reid C. Van Lehn<sup>1,\*</sup>, Manos Mavrikakis<sup>1,\*</sup>

<sup>1</sup>Department of Chemical and Biological Engineering, University of Wisconsin-Madison, Madison, Wisconsin 53706, United States

<sup>2</sup>Smith School of Chemical and Biomolecular Engineering, Cornell University, Ithaca, New York 14853, United States

<sup>3</sup>Department of Civil and Environmental Engineering, University of Wisconsin-Madison, Madison, Wisconsin 53706, United States

**KEYWORDS:** liquid crystals, chemoresponsive systems, density functional theory, molecular dynamics, anchoring energy, and elastic energy.

ABSTRACT: Computational chemistry calculations are broadly useful for guiding the atom-scale design of hard-soft material interfaces, including how molecular interactions of single-component liquid crystals (LCs) at inorganic surfaces lead to preferred orientations of the LC far from the surface. The majority of LCs, however, are not single-component phases but comprise mixtures, such as mixture of mesogens, added to provide additional functions such as responsiveness to the presence of targeted organic compounds (for chemical sensing). In such LC mixtures, little is understood about the nearsurface composition and organization of molecules, and how that organization propagates into the far-field LC orientation. Here, we address this broad question by using a multi-scale computational approach that combines density functional theory (DFT)-based calculations and classical molecular dynamics (MD) simulations to predict the interfacial composition and organization of a binary LC mixture of 4'-cyano-4-biphenylcarbolxylic acid (CBCA) and 4'-n-pentyl-4-biphenylcarbonitrile (5CB) supported on anatase(101) titania surfaces. DFT calculations determine the surface composition and atomic-scale organization of CBCA and 5CB at the titania surface, and classical MD simulations build upon the DFT description to describe the evolution of the near-surface order into the bulk LC. A surprising finding is that the 5CB and CBCA molecules adopt orthogonal orientations at the anatase surface, and that above a threshold concentration of CBCA, this mixture of orientations evolves away from the surface to define a uniform far-field homeotropic orientation. These results demonstrate that molecular-level knowledge achieved through a combination of computational techniques permits the design and understanding of functional LC mixtures at interfaces.

The capability to design liquid crystal (LC) interfaces with desired properties is enabling development of functional materials for use in applications such as gas sensors1, actuators2, liquid crystal displays3, or assays for targeted biological species4. Because LCs are mesophases that contain fluid-like mobility and long-range orientational order,5 the preferred orientation of a LC (the director) within a micrometer-thick film can be controlled by molecular-level interactions at its interfaces<sup>6-17</sup>. The importance of interfacial interactions of LCs has inspired numerous computational and experimental studies to elucidate how molecular order propagates from the interface into the far-field LC orientation (referred to as *anchoring*)<sup>18</sup>. Common approaches to study LC anchoring utilize coarse-grained simulations<sup>19–22</sup> or continuum-scale numerical calculations (e.g., within the Landau-de Gennes theoretical framework) in which an anchoring energy is imposed to orient the LC director at the surface<sup>23-26</sup>. Such simulations do not resolve the relationship between LC-surface interactions, near-surface LC organization, and the resulting far-field LC orientation. To address this challenge, more recently, atomistic molecular dynamics (MD) simulations of single-component LCs have been performed to model LC ordering as a function of the distance from various surfaces and to predict corresponding anchoring energies<sup>27–33</sup>. In addition to focusing on single-component LCs, however, most of the above-described molecular simulations of LCs have calculated anchoring energies that differ from experimental values by orders-of-magnitude<sup>27,28,34</sup>. Some prior studies have focused more broadly on LC mixtures including calculations of structure and transport properties from molecular-scale simulations<sup>35–38</sup>. However, how LC mixtures organize at interfaces, and how the interfacial organization of the mixture propagates into the far-field, is not well-understood and to the best of our knowledge has not been studied using modern computational methods.

One applied context in which the interfacial composition and structure of LC mixtures deposited at substrates is important is the design of chemically-responsive LC materials (termed chemoresponsive LCs in the remainder of this manuscript). Chemoresponsive LCs amplify nanoscale changes in LC interfacial organization<sup>39</sup> triggered by analytes, with the far-field LC organization being transduced optically<sup>1</sup>. For example, chemoresponsive LCs have been developed for the detection of gaseous organophosphorus compounds (*e.g.*, dimethyl methylphosphonate, DMMP)<sup>7–9,34</sup>. These systems utilize the nematic

LC 4'-n-pentyl-4-biphenylcarbonitrile (5CB; structure in Figure 1a), which contains a nitrile group that coordinates strongly to certain metal-salt surfaces and thereby induces 5CB molecules to orient perpendicular to the surface. The near-surface orientation of 5CB propagates from the surface into a far-field homeotropic (*i.e.*, perpendicular to the surface) orientation of the LC film. If a targeted analyte such as DMMP binds more strongly to the metal salt than 5CB, then the analyte molecules can displace bound 5CB mesogens from the surface. The displacement of 5CB drives a local reorientation of the mesogens that propagates into a change in the far-field orientation of the LC film (from homeotropic to parallel orientations)<sup>7,9,34</sup>. For such systems, we have shown that electronic structure calculations using density functional theory (DFT) can be used to relate surface binding energies of mesogens and DMMP to LC anchoring behaviors and LC orientational transitions<sup>7,9,34</sup>. Building from this capability, DFT-based models of single-component LC-surface interactions have been used to design chemoresponsive LCs that exhibit high water tolerance<sup>7</sup>, responses that can be tailored through the choice of anions in the metal salt<sup>34</sup>, responses to oxidizing gases<sup>6,40</sup> and other analytes that dissociate on metal surfaces<sup>39</sup>.

In the computational studies described above pertaining to behaviors of LC mixtures, the LCs were modeled with DFT as single-component systems by focusing only on the component of the LC mixture most abundant at the surface. This simplified view, while insightful, does not consider how the composition of the near-surface region of the LC will depend on interfacial interactions, nor how composition and ordering of the mixture of molecules within the LC will evolve away from the surface to define the far-field orientation of the LC. These considerations are particularly relevant to LC systems composed of mixtures of mesogens and dopants, as the use of dopants permits tuning of the interactions of the LC at the surface while maintaining mesophase properties using the mesogens<sup>6-8,39,41</sup>. For example, we have recently shown that a LC mixture of 5CB and 4'-cyano-4-biphenylcarboxylic acid (CBCA; structure shown in Figure 1a) deposited on the anatase(101) titania (TiO<sub>2</sub>) surface can be used to create chemoresponsive LCs that respond selectively to SO<sub>2</sub><sup>41</sup>. Whereas 5CB adopts a planar orientation on anatase(101), as shown in Figure 1b, adding CBCA as a dopant was found to induce the homeotropic anchoring of 5CB. We determined that the benzoic acid group of CBCA binds strongly to the anatase(101) surface to induce the homeotropic LC orientation. Subsequent exposure of the supported film of LC to humid SO<sub>2</sub> gas resulted in a surface reaction that displaced the bound CBCA molecules from the surface. This displacement triggered a change in the far-field LC orientation and optical detection of SO<sub>2</sub>.

As noted above, the use of a binary LC mixture comprising 5CB and a dopant as a chemoresponsive LC raises fundamental questions relating to surface composition and organization to LC anchoring. From the standpoint of sensor design, understanding the relationship between near-surface LC organization, far-field orientation, and dopant concentration could help design LC mixtures with improved properties. In this work, we investigate these relationships by using a multiscale computational approach that combines first-principles DFT calculations with classical MD simulations to study the adsorption of 5CB and CBCA mixtures at the anatase(101) surface. We utilize DFT calculations to answer questions regarding the near-surface composition and structure of co-adsorbed molecules related to bulk concentrations. MD simulations, informed by DFT, are used to resolve how the surface adsorbate composition influences anchoring energies in the binary LC mixture. In addition, MD simulations show how near-surface 5CB orientations propagate to the bulk LC. Together, this computational approach permits us to answer how dopant concentration affects LC anchoring, enabling comparisons to experimental observations. These findings provide fundamental physical insight into the near-surface structures of co-adsorbed molecules in a binary LC mixture, and showcase an integrated DFT/MD approach to predict anchoring behavior that can guide the design of chemoresponsive LC systems.

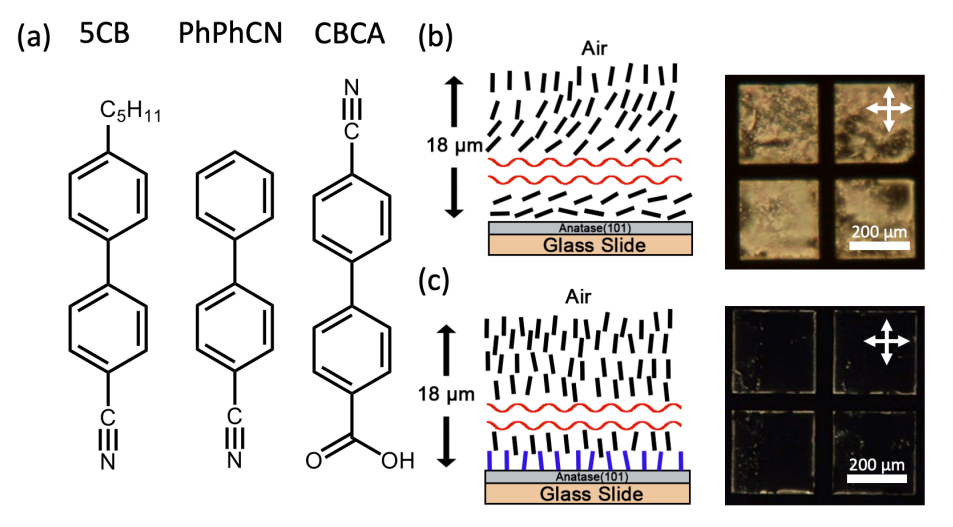


**Figure 1.** (a) Molecular structures of 4'-n-pentyl-4-biphenylcarbonitrile (5CB), 4-biphenylcarbonitrile (PhPhCN; 5CB surrogate), 4'-cyano-4-biphenylcarbolxylic acid (CBCA). (b) and (c) Schematic illustrations of the director profile (left) and optical images (crossed polarizers) of LC hosted in 18  $\mu$ m-thick copper TEM grids (lateral size of grid square is 285  $\mu$ m with white crossed double-headed arrows showing the orientations of the polarizers). Images in (b) show planar anchoring whereas images in (c) show homeotropic anchoring. The short line segments in the schematic illustrations in (b) and (c) represent mesogens. The black-colored line segments indicate bulk mesogens (mostly 5CB) and the violet-colored line segments indicate surface-adsorbed CBCA. The wave-shaped horizontal red-colored lines indicate that the TEM grids contain many more mesogens between the air and anatase interfaces than are shown in the schematic illustrations.

# RESULTS AND DISCUSSION

The primary objective of our work is to develop a multi-scale modeling framework that enables an improved nano-scale understanding of how the organization of LCs comprised of mixtures of mesogens adsorbed at a solid surface evolve away from the surface to define a uniform far-field LC orientation. Such an advance in fundamental understanding has the potential to enable the development of liquid crystalline-based systems with broad potential utility, including as chemoresponsive systems. Our approach is to first calculate the preferred orientations of mixtures of CBCA and 5CB mesogens adsorbed at  $TiO_2$  surfaces at coverages of up to one monolayer using DFT. The DFT-calculated energetically preferred structures are then used to develop MD simulations for understanding how a surface with mixed orientations of CBCA and 5CB influences the LC ordering as a function of distance away from the surface. When combined with a DFT calculated phase diagram, these MD simulations allow us to predict how the concentration of CBCA (the strong binding agent) leads to homeotropic or planar anchoring of the LC in the far-field, a prediction that was subsequently confirmed with experimental evaluation. Overall, this work demonstrates how a combined DFT and MD multi-scale model, starting from nanoscale calculations, can explain behaviors of soft materials in the macroscale.

# Coadsorption of CBCA with 5CB on anatase(101) surfaces as a function of coverage

We first report DFT calculations that build upon our methods used previously for extended surfaces<sup>39</sup>. Here, we consider the effect of surface coverage on the energetically preferred states of 5CB mesogens or CBCA dopants coadsorbed on anatase(101). In these initial calculations, we evaluate possible stable surface structures for 5CB and CBCA adsorbed in perpendicular ( $\bot$ ) orientations. Below, we relax this assumption and allow 5CB and CBCA to adopt a variety of orientations at the anatase surface (we determine the thermodynamically most favorable mixed orientational states of the mixture using DFT). We initially chose to investigate perpendicular orientations because perpendicular orientations are expected to promote homeotropic LC anchoring (bulk LC is perpendicular to the surface) while parallel adsorbates are expected to promote planar anchoring (bulk LC is parallel to the surface)  $^{6,39-41}$ . We study all possible combinations of co-adsorbed CBCA and PhPhCN (5CB surrogate in Figure 1a) on a (2x2) anatase(101) unit cell. We show the most energetically preferred states in Figure 2a for CBCA and PhPhCN co-adsorbed where each slab contains 0.25 ML, 0.50 ML, 0.75 ML, or 1 ML CBCA balanced with PhPhCN to ensure the total coverage of the slab is fixed to 1 ML (5.11 molecules/nm²). The energetics characterizing these structures are shown in Figure 2b as differential binding energies (BE<sub>diff</sub>) of CBCA. As noted in the Introduction, CBCA binds to the anatase surface via its carboxylic acid group. We observed that the BE<sub>diff</sub> of CBCA monotonically decreases in magnitude with increasing coverage of CBCA. For example, the BE<sub>diff</sub> is -2.85 eV for 0.25 ML  $\bot$  CBCA and 0.75 ML PhPhCN,

while the BE<sub>diff</sub> is only -1.95 eV for 1 ML  $\perp$  CBCA. This decrease in the magnitude of the differential BE with coverage is due to destabilizing interactions from electronic effects (as described in the Supporting Information-SI). In addition, these destabilizing interactions between CBCA molecules can be observed from the structure of adsorbed CBCA in Figure 2a where CBCA molecules prefer to adsorb as far as possible from each other for 0.5 ML  $\perp$  CBCA 0.5 ML  $\perp$  PhPhCN case. For this structure, there is a 0.05 eV energy cost to place two CBCA molecules next to each other compared to the preferred state, which is significant because 0.06 eV corresponds to one order of magnitude in surface coverages at room temperature. In addition, this effect can be more significant for larger distances between CBCA molecules. For example, if we consider Equation (1) corresponding to separating CBCA molecules from the 0.50 ML CBCA structure to the 0.25 ML CBCA structure, there is a change in energy of -0.62 eV. Therefore, CBCA molecules strongly prefer to separate from each other on the anatase(101) surface.

$$(\perp 0.50 \ ML \ CBCA \perp 0.50 \ ML \ PhPhCN) + (\perp 1ML \ PhPhCN) \rightarrow 2(\perp 0.25 \ ML \ CBCA + \perp 0.75 \ ML \ PhPhCN)$$
 (1)

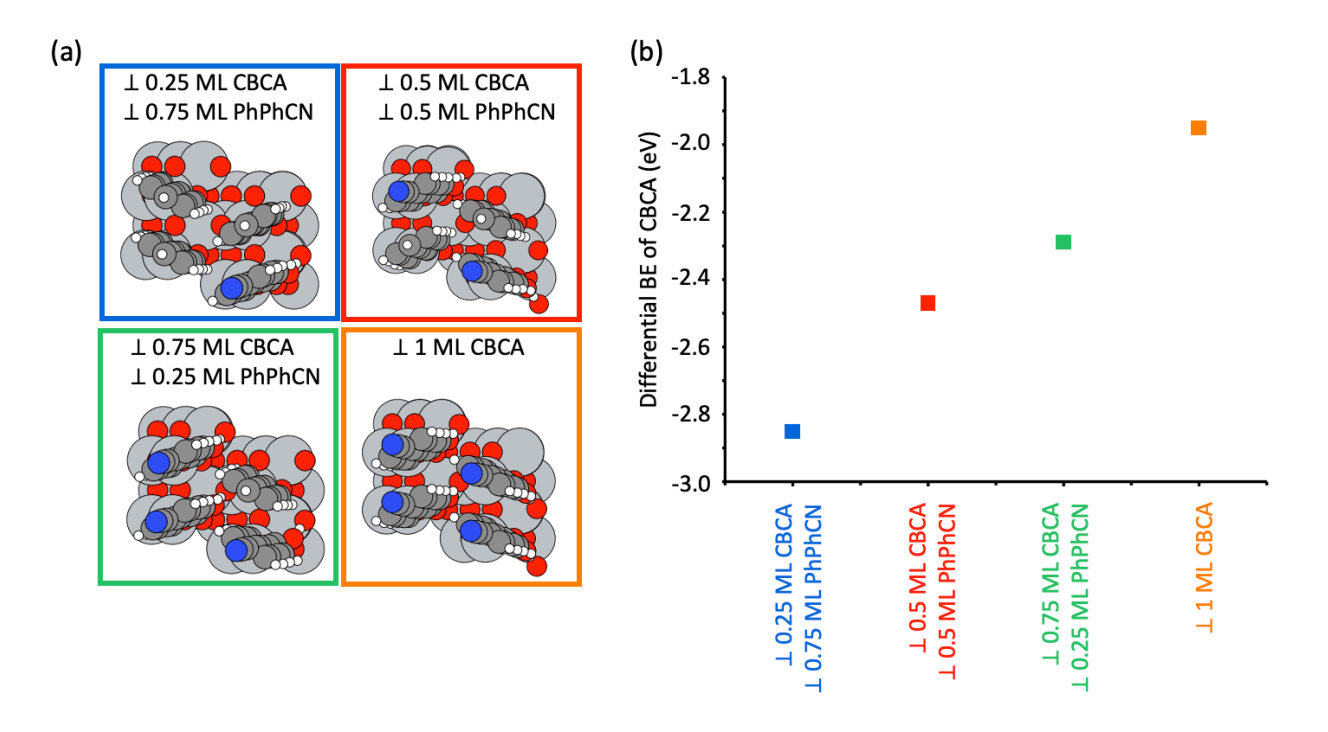


**Figure 2**. (a) Top view of energetically preferred structure of CBCA and PhPhCN co-adsorbed on anatase(101) in perpendicular orientations. White, dark gray, blue, red, and light gray colors indicate H, C, N, O, and Ti atoms, respectively. (b) Calculated  $BE_{diff}$  for one CBCA molecule on anatase(101) when the surface has adsorbed 0.25 ML, 0.50 ML, 0.75 ML, and 1 ML CBCA co-adsorbed with 0.75 ML, 0.50 ML, 0.25 ML, and 0 ML PhPhCN, respectively, all in perpendicular orientations.

The strong  $BE_{diff}$  at low coverages ( $BE_{diff}$  = -2.85 eV; 0.25 ML  $\perp$  CBCA and 0.75 ML  $\perp$  PhPhCN) and also at high coverages ( $BE_{diff}$  = -1.95 eV; 1 ML  $\perp$  CBCA) suggest that CBCA may completely partition to the surface. An important consideration is the destabilization that occurs at higher coverages of CBCA (Figure 2b shown by the decrease in  $BE_{diff}$  with coverage), which may make it unfavorable for CBCA to bind as CBCA coverage increases towards one ML CBCA. It is possible that lower coverages than those shown in Figure 2b may also be favorable, but lower coverages cannot be resolved in the (2x2) anatase(101) unit cell. Therefore, we turn to classical MD simulations to further examine the structure of 5CB and CBCA molecules at low CBCA coverages.

#### Ordering of 5CB near CBCA-adsorbed anatase(101) surfaces using MD simulations

We performed MD simulations to study the structure of 5CB near the anatase(101) surface for CBCA coverages between 0 and 0.24 ML, and we determined if such coverages promote homeotropic anchoring. This coverage range corresponds to the low coverages ( $\leq$  0.25 ML) expected to be more favorable based on the DFT calculations. Simulations were performed using an anatase-anatase system in which two anatase surfaces were modeled, each covered with the same number of adsorbed CBCA molecules and with 5CB molecules occupying the space between the two surfaces (Figure 3a). This geometry models

the sandwich cell setup utilized in our experiments, whereas a system with one anatase surface and one free (i.e., LC-air) interface would instead model the TEM grid-based experiments, also used in separate experiments. Simulating the anataseanatase sandwich cell system eliminates any stored elastic energy that results from differences in the anchoring of 5CB molecules near the anatase surface and a free interface. A challenge in modeling the binary LC mixture is that the bulk concentration of CBCA at experimentally relevant concentrations is very low (<0.1 mol % CBCA; vide infra), so that it is computationally infeasible to model the equilibrium exchange of CBCA molecules between the surface and bulk LC. As discussed below, however, both DFT and experiments reveal that almost all CBCA molecules in the mixtures of CBCA and 5CB used in experiment bind to the anatase, leaving very low concentrations on CBCA in the LC phase. Accordingly, we specified the surface coverage of CBCA molecules in each MD simulation a priori and treated the bulk LC as pure 5CB. To maintain the desired coverage, CBCA molecules were restrained to the surface to prevent any diffusion into the bulk. Restraints were informed by the DFT calculations in two ways. First, a restraint was placed to maintain the position of each adsorbed CBCA molecule relative to atoms at the anatase(101) surface based on the energy-minimizing positions obtained from DFT (Figure 2). In the absence of this restraint, the MD simulations show that CBCA molecules remain adsorbed to the surface in agreement with DFT and experiments. However, this restraint is necessary to prevent the lateral diffusion of CBCA molecules on the surface away from the DFT-identified positions (further discussed in the SI). Second, an angular potential function was applied to the CBCA molecules that was parameterized based on DFT binding energies as a function of the angle between the C-C bond that connects the two phenyl rings of the CBCA molecule and the surface in the absence of 5CB solvation<sup>41</sup>. This potential reaches a minimum for a perpendicular CBCA orientation for 0.25 ML CBCA in vacuum (additional details are included in the SI). Together, these two potentials ensured a near-surface CBCA structure that models findings from DFT; further analysis of simulations without restraints is included in the SI. 5CB molecules were not restrained to permit exchange with 5CB molecules in the bulk LC and their preferred orientations were determined from the simulations. This approach is informed by the known weak interaction of 5CB with the anatase(101) surface<sup>41</sup>.

Following prior MD studies of 5CB structure near interfaces<sup>27,31,32</sup>, we analyze LC structure by computing an order parameter,  $P_2$ , that quantifies the average orientation of 5CB molecules relative to the surface normal as a function of the distance from a single anatase surface projected onto the z-axis (z), as defined by Equation 2:

$$P_2(z) = \langle \frac{3}{2}\cos^2\theta - \frac{1}{2} \rangle_z \tag{2}$$

In this equation,  $\theta$  is the angle of the molecular axis of a 5CB mesogen with respect to the z-axis and is calculated for each mesogen separately, then  $P_2(z)$  is computed by histogramming z in increments of 0.1 nm and averaging over all mesogens within each bin and all frames of the trajectory. We emphasize that  $P_2$  is not the scalar order parameter commonly used to assess the alignment of mesogens relative to the local director, since  $\theta$  is defined relative to the surface normal and not the local director. Instead,  $P_2=1$  indicates that 5CB molecules are oriented perpendicular to the surface on average and  $P_2=-0.5$  indicates that 5CB molecules are oriented parallel to the surface. Figure 3b shows  $P_2(z)$  for coverages of CBCA between 0 and 0.24. For 0 ML coverage of CBCA,  $P_2$  is negative for all values of z, indicating that the MD simulations predict parallel orientations of 5CB molecules near the surface, in agreement with DFT calculations (Figure S3), and in the bulk LC (defined as the region several nanometers from the surface where  $P_2$  plateaus). This result is consistent with experimental observations of planar anchoring of 5CB on anatase(101) in the absence of CBCA (Figure 1b). For 0.06 ML and 0.12 ML coverages of CBCA, there is a small increase in  $P_2$  near each surface but  $P_2$  remains negative for all values of z. For 0.18 ML and 0.24 ML coverages of CBCA,  $P_2$  is negative close to the surface before increasing to positive values near z=2 nm.  $P_2$  maintains a positive value with only small oscillations (also observed in previous simulations of the LC-air interface<sup>32</sup>) for all z values more than 2 nm away from either anatase surface. The positive values indicate that there is a threshold CBCA coverage above which homeotropic LC anchoring is achieved.

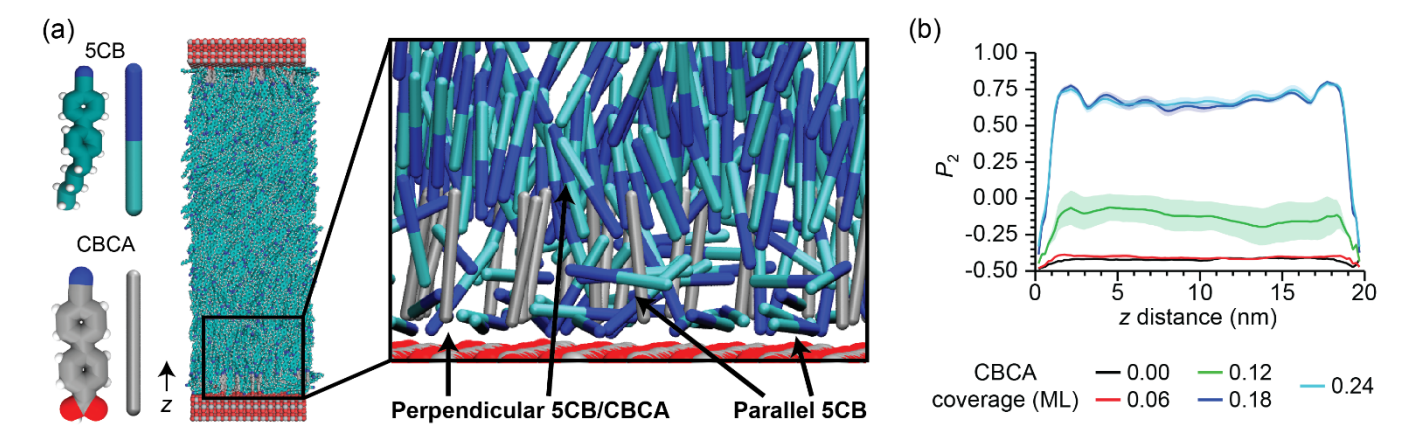


**Figure 3.** (a) Snapshots from MD simulations of sandwich cells comprised on two anatase surfaces covered with 0.24 ML CBCA. The two surfaces are separated by 24.8 nm and images at left illustrate the color scheme. The image at right further elucidates the near-surface organization of the LC mixture, showing both parallel and perpendicular orientations adopted by 5CB molecules but homeotropic anchoring at farther distances from the surface. In this image, the two molecules are shown as "rods" as illustrated at left to visualize their molecular orientations more clearly. (b) Order parameter quantifying the average orientation of 5CB molecules relative to the surface normal as a function of the distance from one anatase substrate (z as indicated in part a) in an anatase-anatase sandwich cell system. Each line corresponds to a different monolayer coverage of CBCA. Lines and shaded regions report averages and standard deviations computed from three independent simulation replicas. Positive values indicate perpendicular orientations relative to the surface, negative values indicate parallel orientations relative to the surface.

For all coverages of CBCA, P2 is negative at distances less than 1 nm from the surface, indicating that 5CB molecules prefer parallel orientations. Conversely, calculations of the  $P_2$  order parameter for CBCA molecules indicate that they exhibit largely perpendicular orientations ( $P_2 \approx 0.8$ -0.9) for all ML coverages (see SI, Figure S12); we note that the angle potential (parameterized from DFT) permits parallel orientations of CBCA in the presence of 5CB, but such orientations are rare. Together, these analyses indicate that 5CB molecules adopt parallel orientations even when co-adsorbed CBCA molecules exhibit perpendicular orientations. Above the threshold CBCA coverage, these mixed orientations promote homeotropic anchoring in the bulk LC. This behavior is observable in the simulation snapshots shown in Figure 3a; some 5CB molecules near the surface assume parallel orientations between adsorbed CBCA molecules, but 5CB molecules farther from the surface are perpendicular on average (snapshots for each ML coverage are shown in SI Figure S14). Our hypothesis is that, near the surface, 5CB adopts parallel orientations due to weak binding of the nitrile group to the anatase surface, which is mostly from electrostatic interactions. Farther from the surface, 5CB is oriented by the tail nitrile group of the CBCA molecule to exhibit homeotropic ordering. An analogous, but opposite phenomenon, has been observed in prior MD simulations of 5CB ordering near alkane self-assembled monolayers in which 5CB molecules exhibited perpendicular orientations near the surface due to interdigitation within the monolayer but planar ordering far from the surface<sup>31</sup>. These results emphasize that the orientations of mesogens near a surface are not necessarily equivalent to their orientations in the bulk LC, leading to mixed orientations in co-adsorbed 5CB and CBCA molecules that are difficult to predict. The MD simulations further indicate that, at low CBCA coverages, co-adsorbed molecules in mixed orientations can still anchor the bulk LC in a homeotropic configuration if sufficient CBCA is adsorbed to the substrate, indicating that the destabilizing interactions that favor low CBCA coverages do not inhibit homeotropic anchoring.

#### Predicting the most favorable surface structures as a function of CBCA concentration

Due to the low dopant concentrations present in the experimental system, the MD simulations described above were performed by specifying the surface coverage of adsorbed CBCA molecules a priori. Thus, the MD simulations do not directly provide information on the equilibrium CBCA coverage as a function of bulk CBCA concentration. The equilibrium CBCA coverage can instead be determined by the calculation of surface free energies, referenced to the vapor pressure of CBCA, at relevant CBCA coverages and concentrations via additional DFT calculations. To elucidate this effect, we compare the surface free energy of co-adsorbed molecules in perpendicular, parallel, and mixed orientations as a function of CBCA concentration in mixtures of CBCA and 5CB as shown in Figure 4a. In addition to the structures included in Figure 2a, we also find the parallel PhPhCN structure (|| 0.25 ML PhPhCN) to be favored at certain conditions. We find some of the structures probed are never favored (e.g. || 0.25 ML CBCA) so we only show the most stable structures in Figure 4a, but all structures evaluated are shown in Figure S3. We also include some mixed orientation structures, defined as ⊥ CBCA and || PhPhCN on the same surface, based on the MD simulation findings. We, therefore, include the surface free energies of mixed orientation structures of  $\pm$  0.50 ML CBCA || 0.33 ML PhPhCN (structure in Figure 4a) or ⊥ 0.25 ML CBCA || 0.50 ML PhPhCN (structure in Figure S10) as shown in the surface free energy calculations in Figure 4a. For these mixed ⊥ CBCA and | PhPhCN structures, we add a second solvent-like layer of PhPhCN to fill the cavitation that forms between CBCA molecules. For example, the structure ± 0.50 ML CBCA || 0.33 ML PhPhCN (Figure 4a) contains ⊥ 0.50 ML CBCA || 0.165 ML PhPhCN at the surface with a second layer of || 0.165 ML PhPhCN to fill the cavity (see SI for more details).

We partition Figure 4a into four regions by vertical lines based on the structure that is most thermodynamically stable (more negative surface free energy is more thermodynamically stable). At higher concentrations of CBCA (above 2 mol%, referring to the concentration added as a dopant to the bulk LC), we find that  $\pm 1$  ML CBCA is preferred. However, this concentration is above the solubility limit of CBCA in 5CB that we find from experiments, so this structure is not relevant under our experimental conditions (we find the maximum solubility is around 0.05 – 0.1 mol% CBCA in 5CB). As we further decrease the concentration of CBCA, we find that between 0.1 mol% and 1.5 mol% the mixed perpendicular state  $\pm$  0.75 ML CBCA  $\pm$  0.25 ML PhPhCN is preferred. This concentration is closer to experimentally relevant concentrations but still slightly above the solubility limit. As we further decrease the concentration of CBCA in 5CB to the range of 0.0025 mol% to 0.1 mol%, we find that the mixed orientation  $\pm$  0.5 ML CBCA || 0.33 ML PhPhCN is most favored. These concentrations are more relevant based on CBCA solubility limits in 5CB. As we further decrease the concentration of CBCA to below 0.0025 mol%, we find that

eventually the surface with no CBCA (|| 0.25 ML PhPhCN) is preferred. These results indicate that the  $\pm$  1 ML CBCA structure is never favored under experimentally relevant concentrations of CBCA.

Typically, when using DFT, phase diagrams are formulated by just showing the lowest surface free energy state, but this can be misleading<sup>42</sup> including the example here. To demonstrate this problem, we calculate at low concentrations of CBCA from 0.0025 mol% to 0.005 mol% that the ⊥ 0.50 ML CBCA || 0.33 ML PhPhCN structure is most favored. However, under this concentration range in experiments with 18 µm-thick CBCA-5CB mixtures supported on one anatase(101) surface (TEM grid setup), there are insufficient CBCA molecules in solution to adsorb at a coverage of 0.50 ML of CBCA. This implies that the equilibrated concentration of CBCA is very different from the concentration of CBCA present in each CBCA and 5CB mixture prepared initially for experiments. This means a large fraction of CBCA molecules in the mixture adsorb to the surface due to the small reservoir of CBCA molecules. We resolve this issue by iterating over CBCA concentration (procedure described in the SI) to determine the equilibrated CBCA concentrations, but the reported concentrations in Figure 4a are the initial concentration of CBCA used in experiments for LCs confined in an 18 µm-deep well. During this iterative process, we calculate occupancy probabilities as reported in Figure 4b. As we decrease CBCA coverage below 0.5 ML, we find an increase in the surface fraction covered by parallel PhPhCN with only two structures dominating: no CBCA (|| 0.25 ML PhPhCN) and 0.50 ML CBCA (± 0.5 ML CBCA || 0.33 ML PhPhCN) structures. These findings are in good agreement with the MD simulations which predicted parallel 5CB orientations near the anatase surface for low CBCA coverages, which is consistent with a combination of parallel PhPhCN orientations and mixed-orientation structures. We also observed a similar effect at higher concentrations where the monolayers of CBCA can be essentially calculated as an interpolation between the two structures  $\perp$  1 ML CBCA and  $\perp$  0.75 ML CBCA  $\perp$  0.25 PhPhCN.

To summarize, the first goal of this combined DFT and MD coverage study was to determine how the near surface ordering of 5CB and CBCA propagates into the far-field orientation of the LC. A key finding of our calculations is that the preference for mixed orientation structures in most experimentally relevant concentrations cannot be easily related to bulk LC anchoring. For example, at 0.50 ML CBCA, we find the mixed orientation structure is calculated to be preferred ( $\pm$  0.50 ML CBCA || 0.33 ML PhPhCN), and at lower concentrations the surface will contain increasingly less perpendicular CBCA until there are no perpendicular CBCA molecules at the surface as shown by the occupancy probability plot in Figure 4b. While the initial MD simulations reveal that these mixed orientations can promote homeotropic ordering, further quantitative analysis is required to compare simulation findings to experimental results. Therefore, we use MD simulations to further determine how these mixed perpendicular and parallel surface structures relate to anchoring of LCs observed in experiments for both the anatase-anatase sandwich cell and anatase-free TEM grid setups.

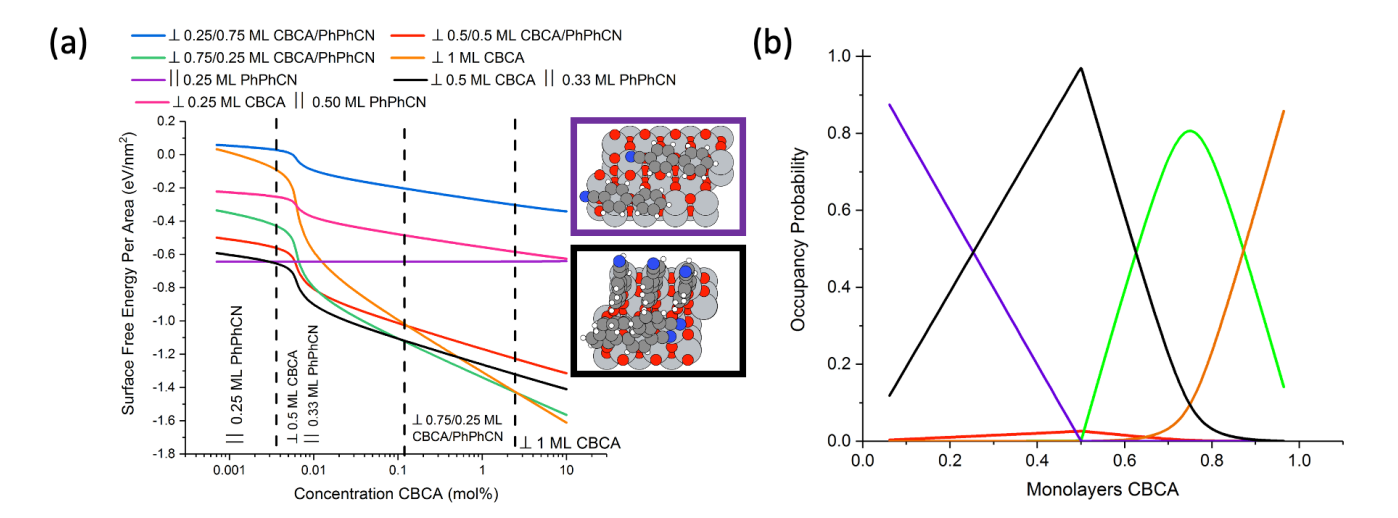


Figure 4. (a) Calculated surface free energies of CBCA and PhPhCN co-adsorbed on anatase(101) as a function of CBCA concentration in 5CB. The calculations were performed for 18  $\mu$ m-thick films of the LC mixtures supported on a single anatase(101) surface (TEM grid setup). Concentration on the x-axis refers to the initial concentration of CBCA (rather than equilibrated concentration) in 5CB, which means this figure depends on the total moles of CBCA in the bulk mixture and, thus, thickness of the LC film. The preferred structure is shown for || 0.25 ML PhPhCN (purple) and the mixed orientation  $\perp$  0.5 ML CBCA || 0.33 ML PhPhCN (black) (b) Occupational probability as a function of monolayer coverage of CBCA on anatase(101) for mixtures of CBCA and PhPhCN. Methodology for calculating these figures is described in the SI (Figure S2). The colors for both figures are defined by the key in (a) where: blue = 0.25 ML  $\perp$  CBCA 0.75 ML  $\perp$  PhPhCN, red = 0.5 ML  $\perp$  CBCA 0.5 ML  $\perp$  PhPhCN, green = 0.75 ML  $\perp$  CBCA 0.25 ML  $\perp$ 

PhPhCN, orange = 1 ML  $\perp$  CBCA, purple = 0.25 ML  $\parallel$  PhPhCN, black = 0.5 ML  $\perp$  CBCA 0.33 ML  $\parallel$  PhPhCN, and pink = 0.25 ML  $\perp$  CBCA 0.50 ML  $\parallel$  PhPhCN.

Predicting anchoring of mixtures of CBCA and 5CB as a function of CBCA concentration

To compare computational results to experimental measurements of the anchoring of mixtures of CBCA and 5CB on anatase, we sought to determine conditions necessary for homeotropic vs. planar anchoring by computing anchoring energies from MD simulations. The magnitude of the anchoring energy quantifies the free energy per unit area required to change mesogen orientations away from a preferred orientation<sup>28,31,43</sup>. Here, we adopt a sign convention in which an anchoring energy is defined as positive if it promotes homeotropic anchoring at a surface (corresponding to a preferred orientation of 0° relative to the surface normal) and negative if it promotes planar anchoring (corresponding to a preferred orientation of 90° relative to the surface normal). We considered both the sandwich cell system with two anatase surfaces and the TEM grid setup supported on a single anatase surface (with the second surface of the LC film being a free surface). The latter geometry, in which the two interfaces are chemically distinct and therefore exhibit different anchoring energies, is representative of typical chemoresponsive LC sensors<sup>39,44</sup>. Nayani *et al.* previously analyzed the LC orientation and stored elastic energies when a LC is confined between two distinct interfaces, one which promotes homeotropic anchoring (*e.g.*, a free surface) and the other which promotes planar anchoring.<sup>43</sup> They showed that the film will adopt a uniform homeotropic orientation when the inequality in Equation 3 is true:

$$-\frac{1}{W_F} - \frac{h}{K} > \frac{1}{W_S} \quad for W_S < 0 \tag{3}$$

where  $W_F$  is the anchoring energy at the free surface (with homeotropic anchoring),  $W_S$  is the anchoring energy at the anatase(101) surface, K is the elastic constant of the LC, and K is the thickness of the LC. Equation 3 is only valid for K0 (planar anchoring favored at the anatase(101) surface) because this condition causes elastic energy to be stored in the LC due to a difference in the preferred director vectors between the anatase surface and the free interface (K0). The LC will assume a planar configuration if the surface strongly directs the 5CB to the planar configuration (K0), overcoming the elastic energy and anchoring energy at the free interface. However, if K0 is only slightly negative then the system assumes a homeotropic configuration.

Applying Equation 3 directly by computing anchoring energies from MD simulations is challenging because MD simulations systematically overpredict the anchoring energy, potentially by several orders of magnitude compared to electro-optical measurements. For example, previous MD calculations have reported  $W_F = 0.15 \text{ J/m}^2$  and  $-W_S = 10^{-1} - 10^{-2} \text{ J/m}^2$  at a silica surface, but these values are much higher than experimental estimates ( $W_F = 10^{-6} - 10^{-4} \text{ J/m}^2$ ,  $-W_S = 10^{-5} - 10^{-3} \text{ J/m}^2$  at a silica surface<sup>27,45</sup>). We obtained similar values for  $W_F$  in a previous study<sup>28</sup> (following the approach discussed below). This overprediction is likely because anchoring energies are calculated in MD simulations using nm-thick LC films whereas in experiments that LC films are micrometers in thickness. Similar conclusions have been reported for experiments using 5CB confined to < 16 nm silica pores where 5CB has a stronger nematic ordering near the interface when compared to bulk 5CB<sup>46</sup>. This pore size is commensurate with the length scale of our MD simulations (24.8 nm separation between slabs), suggesting that the simulations are also influenced by the much smaller length scale modeled compared to the 18  $\mu$ m LC films studied experimentally. Likewise, past experimental studies have shown that anchoring energies scale inversely with LC film thickness, indicating that the anchoring energy should be substantially higher for the systems explored by MD<sup>47</sup>.

To account for this systematic error, we calculated the ratio of the anchoring energy on the anatase (101) surface and the free interface ( $W_S/W_F$ ), which we denote as the relative anchoring energy. We hypothesize that calculating the relative anchoring energy will lead to cancellation of errors associated with the length scale of the MD simulations by estimating values of  $W_S$  and  $W_F$  using systems of comparable size while preserving differences between  $W_S$  due to variations in CBCA coverage. Equation 4 then defines the threshold relative anchoring energy required for homeotropic anchoring, ( $W_S/W_F$ )<sub>threshold</sub>, as the relative anchoring energy required for Equation 6 to be an equality assuming that  $W_S < 0$ :

$$\left(\frac{W_s}{W_F}\right)_{\text{threshold}} = -\frac{1}{\left(\frac{hW_F}{K} + 1\right)} \tag{4}$$

Based on experimental values for the ratio K/h ( $10^{-5}$  J/m² for an 18 µm thick 5CB film) and  $W_F$  ( $5\times10^{-6}-2\times10^{-4}$  J/m²),  $^{43,45}$  the threshold relative anchoring energy is between -2/3 and -1/2. If  $W_s > 0$ , there is no elastic energy stored within the LC and we predict the system to be homeotropic. Therefore, for the TEM grid setup, planar anchoring is predicted when the relative anchoring energy is less than -2/3 (using the more conservative value) and homeotropic anchoring is predicted when the relative anchoring energy is greater than -2/3. We can similarly apply this analysis to predict anchoring in the anatase-anatase sandwich cell system. For this case, there is no elastic energy stored in the LC for any given anchoring energy because

anchoring at both interfaces can be the same. Therefore, homeotropic anchoring is predicted when  $W_s > 0$  and planar anchoring is predicted when  $W_s < 0$ , as the system will align to the direction imposed by the surface.

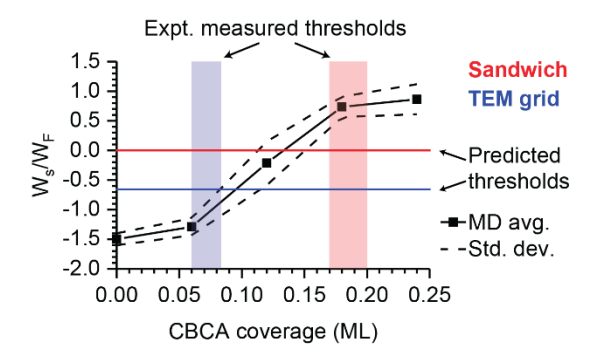


**Figure 5.** MD-predicted relative anchoring energies ( $W_s/W_F$ ) as a function of CBCA coverage. Black solid points and dashed lines report averages and standard deviations, respectively, computed by treating each surface in the anatase-anatase system independently in three MD simulations, which amounts to six total data points. The blue horizontal line shows the threshold relative anchoring energy for a LC film supported on a single anatase surface (TEM grid system; see Eq. 4), whereas the horizontal red line shows the threshold relative anchoring energy for the sandwich cell system comprised of two anatase surfaces. The vertical blue bar shows the range of experimentally measured threshold coverages of CBCA for the TEM grid system and the vertical red bar shows the range of experimentally measured threshold coverages of CBCA for the sandwich-cell system.

To apply Equation 4, we use MD simulations to estimate  $W_3$  and  $W_F$ . Following the procedure of Roscioni *et al*, the anchoring energy was quantified by fitting the probability distribution of  $\theta$  (as defined for Equation 2) to Equation 5<sup>31</sup>:

$$\widetilde{W}_{RP}(z,\cos\theta) = w_0(z) - \frac{1}{2}W(z)\sin^2[\theta - \theta_{eq}(z)]$$
 (5)

where z is the distance from the surface (anatase or free interface) projected onto the z-axis,  $\widetilde{W}_{RP}$  is the effective Rapini-Papoular potential computed from Boltzmann inversion of the probability density at a given z and  $\theta$ ,  $\theta_{eq}(z)$  is the local director for a particular value of z, and the coefficients, W(z) and  $w_0(z)$ , are fit based on the distribution of  $\theta$  as a function of the distance from the surface (discussed in the SI). We define  $W_s$  as the average value of W(z) between z=0 and z=3 nm for the anatase-anatase sandwich cell system. Likewise, we compute  $W_F$  as the average value of W(z) between z=0 and z=3 nm for a two-sided free interface (free-free) system. Figure S13 in the SI reports values of  $W_s/W_F$  for different ranges of z to show the sensitivity of these calculations to the range of z-values used in the calculation.

Figure 5 shows the relative anchoring energy calculated from the MD simulations for low CBCA coverages (which are thermodynamically preferred according to DFT analysis). For 0 ML coverage of CBCA,  $W_S/W_F < -1$ , indicating that planar anchoring is strongly favored. For 0.06 ML CBCA,  $W_S/W_F = -1.2 \pm 0.14$ , which is below the -2/3 threshold, indicating that planar anchoring still occurs for very low CBCA coverages. The relative anchoring energy increases with CBCA coverage and reaches values greater than zero for 0.18 ML (0.73 ± 0.17) and 0.24 ML (0.86 ± 0.25). We thus predict that coverages above 0.18 ML will strongly favor homeotropic anchoring, even in the absence of an air interface. Based on these MD calculations, we predict that the transition from planar to homeotropic anchoring for the CBCA-5CB mixture hosted in an 18  $\mu$ m-thick TEM grid occurs when the coverage of CBCA is between 0.06 ML and 0.12 ML, coverages for which the relative anchoring energy is close to the -2/3 threshold value. We predict that the transition from planar to homeotropic anchoring for 18  $\mu$ m-thick sandwich cell system occurs when the coverage of CBCA is between 0.12 ML and 0.18 ML, for which the relative anchoring energy crosses the threshold value of 0. These predictions can be compared to experimental observations by using input from DFT to relate bulk CBCA concentrations to equilibrium surface coverages to determine the threshold CBCA coverage for homeotropic anchoring, as discussed in the next section.

#### Determination of coverage of CBCA needed for homeotropic anchoring from experiments and DFT

To experimentally determine the threshold coverage of CBCA ( $\theta_{thresh}$ ) on the anatase surface needed for homeotropic anchoring, we confined CBCA-5CB mixtures between two anatase surfaces (anatase-anatase sandwich cell geometry, Figure 6b). We manipulated both the concentration of CBCA ( $C_{CBCA}$ ) and the distance between the two anatase surfaces (d) to change the total number of CBCA molecules per unit area defined as  $C_{2D,CBCA}$  ( $C_{2D,CBCA}$  =  $C_{CBCA}$  × d) in CBCA-5CB mixtures. Experimentally determined values of  $C_{2D,CBCA}$  can then be compared to the CBCA coverages ( $\theta_{CBCA}$ ) predicted from MD simulations by using DFT-calculated surface free energies as shown by the plot in red in Figure 6a for an 18  $\mu$ m-thick TEM grid. For convenience, we describe  $C_{2D,CBCA}$  in unit of molecules in solution per Ti site (or units of monolayers). If all CBCA

molecules in solution adsorb to the surface, then  $C_{2D,CBCA} = \theta_{CBCA}$  (the black dashed line in Figure 6a). We predict from DFT that for  $C_{2D,CBCA}$  less than 0.5 ML, essentially all molecules in solution adsorb. For  $C_{2D,CBCA}$  greater than 0.5 ML, it becomes much more difficult to add CBCA molecules to the surface due to destabilizing interactions and  $C_{2D,CBCA}$  no longer equals  $\theta_{CBCA}$ .

We can further compare DFT-calculated coverage ( $\theta_{CBCA}$ , Figure 6a) to experiments (Figure 6c) to determine  $\theta_{thresh}$  by directly determining the threshold  $C_{2D,CBCA}$  needed for homeotropic anchoring ( $C_{2D,thresh}$ ; where  $C_{2D,thresh}$  =  $C_{thresh}$  × d) from experiments. If essentially all the CBCA molecules in CBCA-5CB adsorb on the anatase surface,  $C_{2D,thresh}$  will equal  $\theta_{thresh}$ . Additionally, we assume that  $\theta_{thresh}$  is not LC-thickness-dependent. This means that if, and only if, all CBCA molecules adsorb to the surface, then Equation 6 holds.

$$C_{2D,thresh} = \theta_{thresh} = constant = C_{thresh} \times d$$
 (6)

where  $C_{thresh}$  would be inversely related to distance d between the two surfaces of the sandwich cell if all CBCA molecules adsorb to the surface. Inspection of Figure 6c reveals that  $C_{thresh}$  was  $0.007\pm0.001$ ,  $0.010\pm0.001$ , or  $0.022\pm0.002$  mol% for d = 18  $\mu$ m, 10  $\mu$ m, or 4  $\mu$ m, respectively. This inverse relationship between  $C_{thresh}$  and LC thickness ( $C_{2D,thresh}$  values are comparable as shown in Figure 6c) indicates that most of the CBCA molecules in the CBCA-5CB adsorb on the anatase surface.

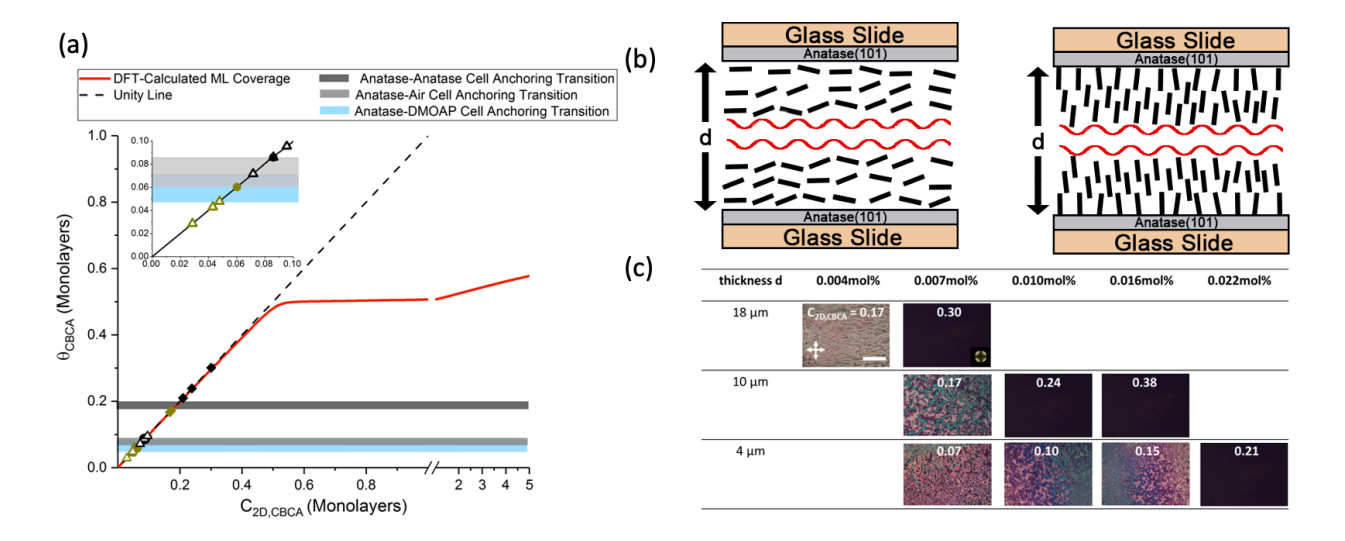


**Figure 6.** (a) The red line is the DFT-calculated monolayer coverage of CBCA ( $\theta_{CBCA}$ ) as a function of CBCA molecules in the CBCA-5CB mixture per Ti site (C<sub>2D,CBCA</sub>) for an 18 μm-thick film of LC supported on a single anatase surface (TEM grid system; all other configurations overlap for  $C_{2D,CBCA} < 0.5$  as described in the SI). We plot the unity line (dashed line), which represents the case if all molecules in the bulk CBCA-5CB mixture were adsorbed on the anatase surface. We also plot experimental data points (filled anatase-anatase sandwich cell, triangle for open an anatase-dimethyloctadecyl[3-(trimethoxysilyl)propyl]ammonium chloride (DMOAP) sandwich cell, and filled circle for a TEM grid sample. The color of the filled diamond, open triangle, or filled circle are either yellow for planar anchoring or black for homeotropic anchoring observed in experiments. We note there are two points that overlap at 0.085 ML (filled black circle and open black triangle). We provide an inset to enlarge the 0 to 0.1 ML region in the upper left corner. The horizontal dark grey, light grey, and blue regions represent the threshold coverage of CBCA needed for homeotropic anchoring ( $\theta_{\text{thresh}}$ ) for anatase-anatase sandwich cell, TEM grid (anatase-air), and anatase-DMOAP sandwich cell, respectively. (b) Schematic illustrations of the director profile of LCs in sandwich cells which have two anatase surfaces for planar (left) and homeotropic (right) LC anchoring, (c) Optical micrographs (crossed polarizers) of CBCA-5CB mixtures with varying CCBCA (black top row) confined in sandwich cells (two anatase surfaces) with LC film thickness of d.  $C_{2D,CBCA}$  is overlaid in white on each image, and the scale bar is 500  $\mu$ m.

In Figure 6a, we compare the experimentally measured  $C_{2D,thresh}$  values for the anatase-anatase sandwich cell geometry (diamonds) to estimate  $\theta_{thresh}$  calculated from DFT. We found that the average value of  $\theta_{thresh}$  is  $\sim$ 0.2 ML (the dark grey region). We find, in agreement with the inverse relationship between  $C_{thresh}$  and d, that DFT predicts all of the CBCA molecules to adsorb to the surface at  $C_{thresh}$ . For the 18 µm-thick TEM grid setup,  $C_{thresh}$  is only 0.001 mol% and  $\theta_{thresh}$  is  $\sim$ 0.06 ML (the light grey region Figure 5a). This TEM grid threshold is smaller than the threshold for the sandwich cell of  $\sim$ 0.2 ML. Unlike the sandwich cell geometry, the TEM grid setup allows the LC to have one free interface with air. The decrease in  $\theta_{thresh}$  found for the TEM grid setup compared to the sandwich cell setup may result from a stronger anchoring energy on the LC-air interface than that on the LC-anatase interface at this coverage of CBCA, which was hypothesized in the MD calculations above. To evaluate this hypothesis for the effect of anchoring energy at interfaces on  $\theta_{thresh}$ , we evaluated the anchoring of CBCA-5CB

sandwich cells consisting of one anatase surface and one dimethyloctadecyl[3-(trimethoxysilyl)propyl]ammonium chloride (DMOAP) adsorbed surface (Figure S11 for anatase-DMOAP sandwich cell). The DMOAP adsorbed surface can provide a strong homeotropic anchoring for 5CB.<sup>48</sup> We found that the average value of  $\theta_{\text{thresh}}$  for DMOAP-anatase cells is ~0.06 ML (Figure 6a in blue), which is similar to  $\theta_{thresh}$  for the 18 µm-thick TEM grid setup. This is likely due to the anchoring energy of DMOAP being of the same order of magnitude as that of the free interface, thus storing a comparable amount of elastic energy. Therefore, sandwich cells with anatase and a surface with a stronger anchoring energy would decrease  $\theta_{thresh}$  needed on the anatase.

These results compare well to MD determined  $\theta_{thresh}$  derived from DFT structures. For the anatase-anatase sandwich cell system, the experimental  $\theta_{thresh}$  is  $\sim$ 0.2 ML, which is similar to the MD calculated value of 0.12 - 0.18 ML (Figure 5). For the anatase-free TEM grid setup, the experimental  $\theta_{thresh}$  is lower with a value of  $\sim$ 0.06 ML due to the anchoring energy of the free interface. This agrees very well with the MD calculated value of 0.06 ML – 0.12 ML, demonstrating that accurate modeling of LC interfaces can be used to directly determine LC anchoring for co-adsorbed mixtures of mesogens and dopants from first principles.

#### CONCLUSION

We report a combined computational chemistry (DFT), molecular dynamics (MD), and experimental approach that develops a detailed nano-scale understanding of a chemoresponsive LC system containing mixtures of mesogens. We detail the surface composition and molecular-scale ordering of CBCA-5CB adsorbed on anatase(101) TiO2 where we find a complex pattern of perpendicular CBCA and parallel 5CB molecules is favored. DFT alone can make accurate predictions of the ordering of mesogens adsorbed on solid surfaces<sup>6,7,39,40</sup>. However, our example shows how MD simulations can be used to describe how the nano-scale orientational patterning of co-adsorbed molecules propagates to optical-scale anchoring observations in experiments by elucidating the relationship between surface free energy and anchoring energy. In agreement with experiments, we find that, depending on the elastic energy imposed on the system, only about 0.06-0.20 ML CBCA in 5CB deposited on anatase(101) is needed for homeotropic anchoring. These results suggest that other LC systems may also contain mixed surface orientations, especially when homeotropic anchoring is achieved with low coverages of strongly bound species. Examples of such systems include: (1) CBCA-5CB on Au (>0.06 mole CBCA per mole Au)<sup>39</sup> or (2) 5CB on Pd-Au alloys (> 0.07 ML of Pd on Au)<sup>49</sup>. When combined, these computational findings provide physical insight into the structure of coadsorbed mixtures of mesogens and dopants and how near-surface structure dictates LC ordering observed in experiments. The results also indicate that decreasing the ratio between  $\theta_{CBCA}$  and the threshold coverage of CBCA needed for homeotropic anchoring  $(\theta_{thresh})$  can permit the design of chemoresponsive LCs that respond to lower concentrations of analytes. Finally, the ability of the combined DFT/MD computational approach to predict experimental anchoring conditions indicates the possibility of utilizing computational modeling to identify LC mixture compositions for alternative sensing applications.

# **METHODS**

# DFT Methods

Bulk, surface, and cluster calculations were performed using Density Functional Theory (DFT) as implemented in the Vienna Ab Initio Simulation Package (VASP). $^{50,51}$  Projected augmented wave potentials were used to describe the electron-ion interactions. $^{52,53}$  The exchange-correlation functional was described by the generalized gradient approximation (GGA-PBE). $^{54}$  All calculations employed Grimme's D3 empirical dispersion correction scheme with zero damping. $^{55}$  Spin polarization had no influence on the total energies for the calculations presented here. The electron wave function was expanded using plane waves with an energy cutoff of  $400 \, \text{eV}$ . The Brillouin zone (BZ) was sampled using  $\Gamma$ -centered Monkhorst–Pack k-point mesh $^{56}$  with a k-point density greater than 11x11 k-points per 1/Å. For example, on (2x2) unit cell of anatase(101) with dimensions of  $11.0 \, \text{Å} \times 7.6 \, \text{Å}$ , we used a k-point mesh of  $1 \times 2 \times 1 \, \text{per unit cell}$ . Gaussian smearing of  $0.1 \, \text{eV}$  was used in all calculations. Structures were relaxed until the Hellmann–Feynman forces acting on each atom were less than  $0.02 \, \text{eV} \, \text{Å}^{-1}$ . Dipole corrections were applied in the direction normal to the surface. $^{57}$ 

Surface models of the anatase  $TiO_2$  surface were constructed using the most stable facet (101). All surface calculations used at least 10 Å of vacuum separating images of each slab in the z-direction. We used a (4x2) and (2x2) unit cell to model all systems in this work. Each slab contained four  $TiO_2$  tri-layers, as used by others in the field<sup>58-60</sup>, with the bottom two  $TiO_2$  layers fixed to the calculated bulk constant of anatase(101)  $TiO_2$ . The calculated lattice constants for anatase (a = 3.80 Å, b = 9.56 Å) were in good agreement with the experimental values (a = 3.78 Å, b = 9.51 Å).

Differential binding energies ( $BE_{diff}$ ) were calculated using Equation 7.

$$BE_{diff} = E_{total} - E_{total - CBCA} - E_{CBCA (gas)}$$
(7)

where  $E_{total}$  is the total energy of the slab including all adsorbates,  $E_{total-CBCA}$  is the total energy of the slab optimized with one less CBCA molecule, and  $E_{CBCA\,(gas)}$  is the energy of a CBCA molecule in the gas phase. By this definition, stronger binding is reflected in a more negative value of BEdiff.

To determine the preferred surface composition and orientation of mixtures of CBCA and 5CB on the surface of anatase, we calculated the surface free energies (γ) as a function of concentration of CBCA in bulk 5CB using Equation 8. In order to model the effect of 5CB co-adsorbed CBCA at the surface, we used the surrogate PhPhCN (Figure 1a) for 5CB in all calculations.

$$\gamma = \frac{G_{\text{total}} - n_{\text{PhPhCN}} \mu_{\text{PhPhCN}} - n_{\text{CBCA}} \mu_{\text{CBCA}} - E_{\text{anatase}}}{A}$$

$$\mu_{O} = G_{O(gas)}^{0} + \Delta G_{sol\nu,O} + K_{B}T ln(X_{O})$$
(9)

$$\mu_O = G_{O(aas)}^0 + \Delta G_{solv,O} + K_B T ln(X_O) \tag{9}$$

where  $G_{total}$  is the total free energy of the slab including all adsorbates,  $n_0$  is the number of organic adsorbates (where  $O = C_{total}$ ) PhPhCN or CBCA) per slab, E<sub>anatase</sub> is the total energy of the adsorbate-free anatase(101) slab, and A is the area of the slab's surface. The chemical potential of each organic molecule, O, in the gas phase  $(\mu_0)$  is defined in Equation 9 in relation to the free energy of the organic molecules in the gas phase at 1 atm ( $G_{0~(gas)}^{0}$ ), the solvation energy of 0 in 5CB ( $\Delta G_{solv,0}$ ), Boltzmann constant ( $K_B$ ), temperature (T), and mole fraction of O in 5CB ( $X_O$ ). We also include the constraint that  $X_{CBCA} = 1 - X_{5CB}$ . These equations assume Raoult's and Henry's Law to relate gas phase energies from DFT to dilute concentrations of CBCA in 5CB. Details about how solvation energies in 5CB were determined are described in the SI.

Gibbs free energies were calculated using the harmonic approximation. The mass-weighted Hessian was built up via numerical differentiation of the energy using a second-order finite difference approach with a step size of 0.008 Å. Vibrational analysis was used to calculate entropies and enthalpies at 300 K.

#### MD Methods

Classical MD simulations were performed using Gromacs 201662 to model the anchoring behavior of mixtures of 5CB and CBCA. 5CB and CBCA molecules were modeled using an all-atom force field, parameterized from previous DFT calculations, which reproduces experimental properties of 5CB near room temperature<sup>36</sup>. The TiO<sub>2</sub> surface was modeled as a slab using previously determined parameters from ab initio simulations of TiO2-water interfaces<sup>63</sup>. We modeled CBCA as adsorbed to TiO<sub>2</sub> based on preferred surface compositions and structures obtained from DFT calculations with mixtures of CBCA and 5CB (see section above). Angle potentials to capture the fluctuations in orientation of adsorbed CBCA molecules were parameterized using DFT calculations as described in the SI and previous work<sup>41</sup>. Force field parameters are included in the Supporting Information. We specified the CBCA surface coverage in MD simulations by first replicating DFT unit cells to create a 5 × 4 grid of unit cells in the x-y plane, leading to 160 CBCA molecules at full monolayer (ML) coverage. We then removed CBCA molecules from these copied unit cells to obtain the preferred coverage predicted by DFT (for a given bulk concentration of CBCA in 5CB). Both DFT predictions and experimental results (described further below) revealed that under the experimentally accessible conditions, all CBCA present in the bulk CBCA and 5CB mixture adsorbs to the surface of the anatase. Accordingly, in our MD simulations, no CBCA molecules are present in the 5CB phase.

The systems of 5CB sandwiched between two CBCA-adsorbed anatase(101) surfaces (anatase-anatase system) were initialized by copying four 5CB systems from previous work, <sup>36</sup> each with dimensions of (6.2 x 6.2 x 6.2) nm<sup>3</sup> and containing 500 5CB molecules, that were initially equilibrated at 27 °C to obtain a nematic phase. The resulting combined system contained 2000 5CB molecules and a length in the z-dimension of 24.8 nm. We extended this simulation box in the zdimension by 3.2 nm when introducing the TiO<sub>2</sub> slab and an additional 1.7 nm when adsorbing CBCA molecules to the slab. A second slab was then added to the system by mirroring the first TiO<sub>2</sub> slab and placing it such that the top of the CBCA layer was 0.1 nm away from the bottom of the 2000-molecule 5CB system. The system was equilibrated with a simulated annealing protocol in which the system was simulated at 227 °C for 5 ns and the temperature was then decreased by 0.66 °C/ns for 300 ns. The system was finally equilibrated at 27 °C for a further 50 ns. The pressure was maintained at 1 bar using a semiisotropic Parrinello-Rahman barostat with a time constant of 2 ps and a compressibility of  $3 \times 10^{-5}$  bar-1. To improve numerical stability, bonds between the adsorbed CBCA molecules and the TiO2 slab were modeled using the pull code feature in Gromacs by replacing the z-position restraint with center-of-mass distance restraint with respect to the nearest TiO2 slab. All simulations used a 2 fs timestep.

# Experimental Methods

Supported micrometer-thick films of LC mixtures with free surfaces were prepared by placing 18 µm-thick copper transmission electron microscopy (TEM) grids (Electron Microscopy Sciences, Hatfield, PA) onto anatase(101) surfaces. The preparation of the anatase(101) surface and mixtures of CBCA and 5CB is described in a previous publication<sup>41</sup>. The TEM

grids possessed square slots with lateral dimensions of 285  $\mu$ m. 0.2  $\mu$ L of a CBCA-5CB mixture was deposited into each TEM grid using a glass capillary. The excess LC was removed from the grid by wicking the LC into an empty capillary tube.

Micrometer-thick films of LCs in sandwich cells were prepared by dispersing fiber spacers with diameters of either 18, 10, or 4  $\mu$ m into Norland Optical Adhesive 65 (Norland Products, Inc., Cranbury, NJ). The perimeters of two anatase (101) surfaces were coated with the adhesive and the surfaces were adhered together by UV exposure for 30 minutes. A drop of CBCA-5CB, heated into its isotropic phase (35.5 °C < T < 40 °C), was then drawn by capillarity into the cavity between the two surfaces of the sandwich cell. The cell was subsequently cooled to room temperature.

# **AUTHOR INFORMATION**

# **Corresponding Author**

\*Corresponding authors: vanlehn@wisc.edu, nla34@cornell.edu, emavrikakis@wisc.edu

### **Author Contributions**

The manuscript was written through contributions of all authors. / All authors have given approval to the final version of the manuscript. / These authors contributed equally. (match statement to author names with a symbol)

#### **ACKNOWLEDGMENT**

This work was supported by the National Science Foundation (Grant Numbers 1837812 and 1837821). The fabrication of  $TiO_2$  surfaces was performed in part at the Cornell NanoScale Facility, an NNCI member supported by NSF Grant NNCI-2025233. Part of the computational work conducted by J. I. G., and M. M. was carried out using computational resources available at the National Energy Research Scientific Computing Center (NERSC) which is supported by the U.S. DOE, Office of Science under Contract No. DE-AC02-05CH11231 using NERSC award BES-ERCAP0022773. Part of the computational work conducted by J. K. S. and R. C. V. used the Extreme Science and Engineering Discovery Environment (XSEDE), which is supported by National Science Foundation grant number ACI-1549562.

# **Supporting Information Available:**

The supporting information provides additional details and methods used for DFT and MD calculations and experimental procedures. This includes further atomic-scale insight into repulsive interactions of adsorbed CBCA molecules using charge density difference calculations. Additional details on parameterization of CBCA angle potential for/with MD and calculations to understand the impact of related assumptions. Images of all relevant DFT structures are provided. Additional details on the fabrication of  $TiO_2$  films are provided.

#### REFERENCES

- (1) Shah, R. R.; Abbott, N. L. Principles for Measurement of Chemical Exposure Based on Recognition-Driven Anchoring Transitions in Liquid Crystals. *Science* (1979) **2001**, 293 (5533), 1296–1299.
- (2) Van Oosten, C. L.; Bastiaansen, C. W. M.; Broer, D. J. Printed Artificial Cilia from Liquid-Crystal Network Actuators Modularly Driven by Light. *Nature Materials* **2009**, *8* (8), 677–682.
- (3) Hoogboom, J.; Rasing, T.; Rowan, A. E.; Nolte, R. J. M. LCD Alignment Layers. Controlling Nematic Domain Properties. *Journal of Materials Chemistry* **2006**, *16* (14), 1305–1314.
- (4) Brake, J. M.; Daschner, M. K.; Luk, Y. Y.; Abbott, N. L. Biomolecular Interactions at Phospholipid-Decorated Surfaces of Liquid Crystals. *Science* **2003**, *302* (5653), 2094–2097.
- (5) Reinitzer, F. Beiträge Zur Kenntniss Des Cholesterins. Monatshefte für Chemie **1888**, 9, 421–441.
- (6) Szilvási, T.; Bao, N.; Nayani, K.; Yu, H.; Rai, P.; Twieg, R. J.; Mavrikakis, M.; Abbott, N. L. Redox-Triggered Orientational Responses of Liquid Crystals to Chlorine Gas. *Angew Chem Int Ed Engl* **2018**, *57* (31), 9665–9669.
- (7) Yu, H.; Szilvási, T.; Rai, P.; Twieg, R. J.; Mavrikakis, M.; Abbott, N. L. Computational Chemistry-Guided Design of Selective Chemoresponsive Liquid Crystals Using Pyridine and Pyrimidine Functional Groups. *Adv Funct Mater* **2018**, *28* (13), 1703581.
- (8) Szilvási, T.; Roling, L. T.; Yu, H.; Rai, P.; Choi, S.; Twieg, R. J.; Mavrikakis, M.; Abbott, N. L. Design of Chemoresponsive Liquid Crystals through Integration of Computational Chemistry and Experimental Studies. *Chemistry of Materials* **2017**, *29* (8), 3563–3571.

- (9) Roling, L. T.; Scaranto, J.; Herron, J. A.; Yu, H.; Choi, S.; Abbott, N. L.; Mavrikakis, M. Towards First-Principles Molecular Design of Liquid Crystal-Based Chemoresponsive Systems. *Nat Commun* **2016**, *7*, 13338.
- (10) Hunter, J. T.; Abbott, N. L. Adsorbate-Induced Anchoring Transitions of Liquid Crystals on Surfaces Presenting Metal Salts with Mixed Anions. *ACS Applied Materials & Interfaces* **2014**, *6* (4), 2362–2369.
- (11) Hunter, J. T.; Abbott, N. L. Dynamics of the Chemo-Optical Response of Supported Films of Nematic Liquid Crystals. Sensors and Actuators B-Chemical 2013, 183, 71–80.
- (12) Wang, P.-H.; Yu, J.-H.; Zhao, Y.-B.; Li, Z.-J.; Li, G.-Q. A Novel Liquid Crystal-Based Sensor for the Real-Time Identification of Organophosphonate Vapors. *Sensors and Actuators B: Chemical* **2011**, *160* (1), 929–935.
- (13) Bungabong, M. L.; Ong, P. Bin; Yang, K.-L. L. Using Copper Perchlorate Doped Liquid Crystals for the Detection of Organophosphonate Vapor. *Sensors and Actuators B: Chemical* **2010**, *148* (2), 420–426.
- (14) Cadwell, K. D.; Lockwood, N. A.; Nellis, B. A.; Alf, M. E.; Willis, C. R.; Abbott, N. L. Detection of Organophosphorous Nerve Agents Using Liquid Crystals Supported on Chemically Functionalized Surfaces. *Sensors and Actuators B: Chemical* **2007**, *128* (1), 91–98.
- (15) Cadwell, K. D.; Alf, M. E.; Abbott, N. L. Infrared Spectroscopy of Competitive Interactions between Liquid Crystals, Metal Salts, and Dimethyl Methylphosphonate at Surfaces. *J Phys Chem B* **2006**, *110* (51), 26081–26088.
- (16) Yang, K.-L.; Cadwell, K.; Abbott, N. L. Use of Self-Assembled Monolayers, Metal Ions and Smectic Liquid Crystals to Detect Organophosphonates. *Sensors and Actuators B: Chemical* **2005**, *104* (1), 50–56.
- (17) Yang, K.-L.; Cadwell, K.; Abbott, N. L. Mechanistic Study of the Anchoring Behavior of Liquid Crystals Supported on Metal Salts and Their Orientational Responses to Dimethyl Methylphosphonate. *Journal of Physical Chemistry B* **2004**, *108* (52), 20180–20186.
- (18) Zannoni, C. From Idealised to Predictive Models of Liquid Crystals. *Liquid Crystals* **2018**, *45* (13–15), 1880–1893.
- (19) Sumer, Z.; Striolo, A. Effects of Droplet Size and Surfactants on Anchoriang in Liquid Crystal Nanodroplets. *Soft Matter* **2019**, *15* (19), 3914–3922.
- (20) Ilnytskyi, J. M.; Trokhymchuk, A.; Schoen, M. Topological Defects around a Spherical Nanoparticle in Nematic Liquid Crystal: Coarse-Grained Molecular Dynamics Simulations. *The Journal of Chemical Physics* **2014**, *141* (11), 114903.
- (21) Zhang, Z.; Guo, H. A Computer Simulation Study of the Anchoring Transitions Driven by Rod--Coil Amphiphiles at Aqueous--Liquid Crystal Interfaces. *Soft Matter* **2012**, *8* (19), 5168–5174.
- (22) Whitmer, J. K.; Joshi, A. A.; Roberts, T. F.; de Pablo, J. J. Liquid-Crystal Mediated Nanoparticle Interactions and Gel Formation. *The Journal of chemical physics* **2013**, *138* (19), 194903.
- (23) Fournier, J.-B.; Galatola, P. Modeling Planar Degenerate Wetting and Anchoring in Nematic Liquid Crystals. *EPL* (*Europhysics Letters*) **2005**, *72* (3), 403.
- (24) Ravnik, M.; Alexander, G. P.; Yeomans, J. M.; Žumer, S. Three-Dimensional Colloidal Crystals in Liquid Crystalline Blue Phases. *Proceedings of the National Academy of Sciences* **2011**, *108* (13), 5188–5192.
- (25) Cavallaro, M.; Gharbi, M. A.; Beller, D. A.; Čopar, S.; Shi, Z.; Baumgart, T.; Yang, S.; Kamien, R. D.; Stebe, K. J. Exploiting Imperfections in the Bulk to Direct Assembly of Surface Colloids. *Proceedings of the National Academy of Sciences* **2013**, *110* (47), 18804–18808.
- (26) Sumer, Z.; Fernandez, F. A.; Striolo, A. Liquid Crystal Droplets under Extreme Confinement Probed by a Multiscale Simulation Approach. *Liquid Crystals* **2021**, *48* (13), 1827–1839.
- (27) Roscioni, O. M.; Muccioli, L. and; Valle, D.; Pizzirusso, A.; Ricci, M.; Zannoni, C.; Industriale, C.; Montanari, T.; Bologna, U.; Bologna, I.-; Della Valle, R. G.; Pizzirusso, A.; Ricci, M.; Zannoni, C. Predicting the Anchoring of Liquid Crystals at a Solid Surface: 5-Cyanobiphenyl on Cristobalite and Glassy Silica Surfaces of Increasing Roughness. *Langmuir* **2013**, *29* (28), 8950–8958.
- (28) Pizzirusso, A.; Berardi, R.; Muccioli, L.; Ricci, M.; Zannoni, C. Predicting Surface Anchoring: Molecular Organization across a Thin Film of 5CB Liquid Crystal on Silicon. *Chem Sci* **2012**, *3* (2), 573–579.
- (29) Ramezani-Dakhel, H.; Rahimi, M.; Pendery, J.; Kim, Y.-K.; Thayumanavan, S.; Roux, B.; Abbott, N. L.; de Pablo, J. J. Amphiphile-Induced Phase Transition of Liquid Crystals at Aqueous Interfaces. *ACS Appl Mater Interfaces* **2018**, *10* (43), 37618–37624.
- (30) Ramezani-Dakhel, H.; Sadati, M.; Rahimi, M.; Ramirez-Hernandez, A.; Roux, B. B.; de Pablo, J. J. Understanding Atomic-Scale Behavior of Liquid Crystals at Aqueous Interfaces. *J Chem Theory Comput* **2017**, *13* (1), 237–244.
- (31) Roscioni, O. M.; Muccioli, L.; Zannoni, C. Predicting the Conditions for Homeotropic Anchoring of Liquid Crystals at a Soft Surface. 4-n-Pentyl-4'-Cyanobiphenyl on Alkylsilane Self-Assembled Monolayers. *ACS Appl Mater Interfaces* **2017**, *9* (13), 11993–12002.
- (32) Sadati, M.; Ramezani-Dakhel, H.; Bu, W.; Sevgen, E.; Liang, Z.; Erol, C.; Rahimi, M.; Taheri Qazvini, N.; Lin, B.; Abbott, N. L.; Roux, B. T.; Schlossman, M. L.; de Pablo, J. J. Molecular Structure of Canonical Liquid Crystal Interfaces. *J Am Chem Soc* **2017**, *139* (10), 3841–3850.

- (33) Chen, H.; Xu, C.; Xiao, G.; Chen, Z.; Yi, M.; Zhang, J. Surface Anchoring Behavior of 5CB Liquid Crystal Confined between Iron Surfaces: A Molecular Dynamics Study. *Appl Surf Sci* **2020**, *508*, 145284.
- (34) Szilvási, T.; Bao, N.; Yu, H.; Twieg, R. J.; Mavrikakis, M.; Abbott, N. L.; Szilvasi, T.; Bao, N.; Yu, H.; Twieg, R. J.; Mavrikakis, M.; Abbott, N. L.; Szilvási, T.; Bao, N.; Yu, H.; Twieg, R. J.; Mavrikakis, M.; Abbott, N. L. The Role of Anions in Adsorbate-Induced Anchoring Transitions of Liquid Crystals on Surfaces with Discrete Cation Binding Sites. *Soft Matter* **2018**, *14* (5), 797–805.
- (35) Rahimi, M.; Ramezani-Dakhel, H.; Zhang, R.; Ramirez-Hernandez, A.; Abbott, N. L.; De Pablo, J. J. Segregation of Liquid Crystal Mixtures in Topological Defects. *Nature communications* **2017**, *8* (1), 1–8.
- (36) Sheavly, J. K.; Gold, J. I.; Mavrikakis, M.; Van Lehn, R. C. Molecular Simulations of Analyte Partitioning and Diffusion in Liquid Crystal Sensors. *Mol Syst Des Eng* **2020**, *5* (1), 304–316.
- (37) Yan, F.; Earl, D. J. Atomistic Simulations of Liquid Crystal Mixtures of Alkoxy Substituted Phenylpyrimidines 2PhP and PhP14. *The Journal of chemical physics* **2012**, *136* (12), 124506.
- (38) Peláez, J.; Wilson, M. Molecular Orientational and Dipolar Correlation in the Liquid Crystal Mixture E7: A Molecular Dynamics Simulation Study at a Fully Atomistic Level. *Physical Chemistry Chemical Physics* **2007**, *9* (23), 2968–2975.
- (39) Yu, H.; Szilvási, T.; Wang, K.; Gold, J. I.; Bao, N.; Twieg, R. J.; Mavrikakis, M.; Abbott, N. L. Amplification of Elementary Surface Reaction Steps on Transition Metal Surfaces Using Liquid Crystals: Dissociative Adsorption and Dehydrogenation. *J Am Chem Soc* **2019**, *141* (40), 16003–16013.
- (40) Bao, N.; Gold, J. I.; Szilvási, T.; Yu, H.; Twieg, R. J.; Mavrikakis, M.; Abbott, N. L.; Szilvasi, T.; Yu, H.; Twieg, R. J.; Mavrikakis, M.; Abbott, N. L. Designing Chemically Selective Liquid Crystalline Materials That Respond to Oxidizing Gases. *J Mater Chem C Mater* **2021**, *9* (20), 6507–6517.
- (41) Bao, N.; Gold, J. I.; Sheavly, J. K.; Schauer, J. J.; Zavala, V. M.; Van Lehn, R. C.; Mavrikakis, M.; Abbott, N. L. Ordering Transitions of Liquid Crystals Triggered by Metal Oxide-Catalyzed Reactions of Sulfur Oxide Species. *J Am Chem Soc* **2022**, *144* (36), 16378–16388.
- (42) Duan, Z.; Henkelman, G. CO Oxidation on the Pd(111) Surface. ACS Catalysis 2014, 4 (10), 3435–3443.
- (43) Nayani, K.; Rai, P.; Bao, N.; Yu, H.; Mavrikakis, M.; Twieg, R. J.; Abbott, N. L. Liquid Crystals with Interfacial Ordering That Enhances Responsiveness to Chemical Targets. *Advanced Materials* **2018**, *30* (27), 1–7.
- (44) Lee, G.; Carlton, R. J.; Araoka, F.; Abbott, N. L.; Takezoe, H. Amplification of the Stereochemistry of Biomolecular Adsorbates by Deracemization of Chiral Domains in Bent-Core Liquid Crystals. *Advanced Materials* **2013**, *25* (2), 245–249.
- (45) Lavrentovich, O. D.; Pergamenshchik, V. M. Stripe Domain Phase of a Thin Nematic Film and the K13 Divergence Term. *Physical Review Letters* **1994**, *73* (7), 979–982.
- (46) Całus, S.; Rau, D.; Huber, P.; Kityk, A. V. Influence of Nanoconfinement on the Nematic Behavior of Liquid Crystals. *Physical Review E Statistical, Nonlinear, and Soft Matter Physics* **2012**, *86* (2), 1–7.
- (47) Ataalla, R. M. S.; Barbero, G.; Komitov, L. Thickness Dependence of the Anchoring Energy of a Nematic Cell. *Journal of Applied Physics* **2013**, *113* (16), 164501.
- (48) Škarabot, M.; Ravnik, M.; Žumer, S.; Tkalec, U.; Poberaj, I.; Babič, D.; Osterman, N.; Muševič, I. Interactions of Quadrupolar Nematic Colloids. *Physical Review E Statistical, Nonlinear, and Soft Matter Physics* **2008**, *77* (3), 1–8.
- (49) Szilvási, T.; Yu, H.; Gold, J. I.; Bao, N.; Wolter, T. J.; Twieg, R. J.; Abbott, N. L.; Mavrikakis, M. Coupling the Chemical Reactivity of Bimetallic Surfaces to the Orientations of Liquid Crystals. *Materials Horizons* **2021**, *8*, 2050–2056.
- (50) Kresse, G.; Furthmüller, J. Efficiency of Ab-Initio Total Energy Calculations for Metals and Semiconductors Using a Plane-Wave Basis Set. *Comput Mater Sci* **1996**, *6* (1), 15–50.
- (51) Kresse, G.; Furthmüller, J. Efficient Iterative Schemes for Ab Initio Total-Energy Calculations Using a Plane-Wave Basis Set. *Phys Rev B Condens Matter Mater Phys* **1996**, *54* (16), 11169–11186.
- (52) Blöchl, P. E. Projector Augmented-Wave Method. Phys Rev B 1994, 50 (24), 17953-17979.
- (53) Kresse, G.; Joubert, D. From Ultrasoft Pseudopotentials to the Projector Augmented-Wave Method. *Phys Rev B Condens Matter Mater Phys* **1999**, *59* (3), 1758–1775.
- (54) Perdew, J. P.; Burke, K.; Ernzerhof, M. Generalized Gradient Approximation Made Simple. *Phys Rev Lett* **1996**, 77 (18), 3865–3868.
- (55) Grimme, S.; Antony, J.; Ehrlich, S.; Krieg, H. A Consistent and Accurate Ab Initio Parametrization of Density Functional Dispersion Correction (DFT-D) for the 94 Elements H-Pu. *J Chem Phys* **2010**, *132* (15), 154104.
- (56) Pack, J. D.; Monkhorst, H. J. Special Points for Brillouin-Zone Integrations. *Phys Rev B* **1977**, *16* (4), 1748–1749.
- (57) Neugebauer, J.; Scheffler, M. Adsorbate-Substrate and Adsorbate-Adsorbate Interactions of Na and K Adlayers on Al(111). *Physical Review B* **1992**, *46* (24), 16067–16080.
- (58) Wang, Y.; Wen, B.; Dahal, A.; Kimmel, G. A.; Rousseau, R.; Selloni, A.; Petrik, N. G.; Dohnálek, Z. Binding of Formic Acid on Anatase TiO2 (101). *The Journal of Physical Chemistry C* **2020**, *124* (37), 20228–20239.

- (59) Langhammer, D.; Kullgren, J.; Österlund, L. Photoinduced Adsorption and Oxidation of SO2 on Anatase TiO2 (101). *Journal of the American Chemical Society* **2020**, *142* (52), 21767–21774.
- (60) Martinez-Casado, R.; Mallia, G.; Harrison, N. M.; Perez, R. First-Principles Study of the Water Adsorption on Anatase (101) as a Function of the Coverage. *The Journal of Physical Chemistry C* **2018**, *122* (36), 20736–20744.
- (61) Horn, M.; Schwerdtfeger, C. F.; Meagher, E. P. Refinement of the Structure of Anatase at Several Temperatures. *Zeitschrift für Kristallographie Crystalline Materials* **2014**, *136* (1–6).
- (62) Abraham, M. J.; Murtola, T.; Schulz, R.; Páll, S.; Smith, J. C.; Hess, B.; Lindahl, E. GROMACS: High Performance Molecular Simulations through Multi-Level Parallelism from Laptops to Supercomputers. *SoftwareX* **2015**, *1*, 19–25.
- (63) Brandt, E. G.; Lyubartsev, A. P. Systematic Optimization of a Force Field for Classical Simulations of TiO2-Water Interfaces. *Journal of Physical Chemistry C* **2015**, *119* (32), 18110–18125.

# For Table of Contents Only

